reactions. This is difficult beyond the maxims that charge localization and separation of opposite charges make solvation more favorable. Consequently, the greater charge separation and increased concentration of charge on the chlorines for **4** as compared to **2** as indicated by the Mulliken populations shown above, suggest that **4** may be better solvated. It is probably best to consider this as a provocative notion since the Mulliken populations are open to criticism.[11] Nevertheless, it does stimulate one to consider what the true reaction pathway is for some common synthetic reactions such as thio ester formation from thiolates and acid halides in dipolar aprotic solvents. In any event, the present results and the related experimental work[1,6] demonstrate that the central role of tetrahedral intermediates in addition reactions is not as universal as commonly assumed.

Acknowledgment. Grati ude is expressed to the National Science Foundation for support of this work.

Supplementary Material Available: Full geometrical details for the acyl halides, ion–dipole complexes, and transition states for reactions 2 and 3 in Z-matrix format (7 pages). Ordering information is given on any current masthead page.

$^4A_2 \rightarrow {}^4T_2$ and $^4A_2 \rightarrow {}^4T_1$ Electronic Transitions in Cobalt(II) Tetrachloride: An FT-IR and Inelastic Electron Tunneling Spectroscopy Study

K. W. Hipps* and Ursula Mazur

Contribution from the Department of Chemistry and Chemical Physics Program, Washington State University, Pullman, Washington 99164-4630. *Received January 2, 1987*

Abstract: The first two electronic transitions in tetraethylammonium cobalt(II) tetrachloride are observed by tunneling spectroscopy. The lowest energy transition [$^4A_2 \rightarrow {}^4T_2$] is electric dipole forbidden, is the most intense transition observed in the tunneling spectrum, and extends from 2000 to 4100 cm^{-1}. The electric dipole allowed $^4A_2 \rightarrow {}^4T_1$ transition is observed in both tunneling and FT-IR spectra and fills the region from 4450 to 7000 cm^{-1}. Significant structuring of this latter band is observed in both FT-IR and tunneling spectra. The inelastic electron tunneling spectroscopy (IETS) results reported are of special significance for several reasons: (a) the magnetic dipole transition is observed with large intensity, (b) significant structure is observed on an electronic transition, and (c) novel data acquisition and analysis techniques are used to extract high-quality electronic spectra from the overall tunneling spectra. We also show that the adsorption of cobalt(II) dichloride on alumina from solution yields (at least in part) surface-supported cobalt(II) tetrachloride ion.

Inelastic electron tunneling spectroscopy (IETS) has proven to be a very sensitive technique for the observation of vibrational spectra.[1-3] While most of the tunneling literature focuses on characterizing chemisorbed species on oxide surfaces, a small group of papers concerns the use of tunneling as a molecular spectroscopy.[4-13] Because the selection rules for IETS are rather weak, vibrational modes which are silent in the IR or Raman, or both, may be directly observed in the tunneling spectrum.[4-8] Thus, when used in concert with IR and Raman spectroscopy, tunneling spectroscopy extends the data base on which assignments may be made and often simplifies the assignment of normal mode frequencies.

Tunneling spectroscopy may also be used to study electronic transitions.[9-13] Electronic transitions in rare-earth oxides,[9,10] phthalocyanine dyes,[9,11] large aromatic molecules,[9] and transition metals[12,13] have been observed by IETS. As a consequence of these studies, it is now known that spin-forbidden transitons ($\Delta S = \pm 1$) occur with intensities similar to spin-allowed transitions. Further, in a recent letter[13] we suggested that magnetic dipole allowed (electric dipole forbidden) transitions might also be observed with significant intensity. Given the richness of the data potentially available from IETS and the large classes of inorganic systems having low energy forbidden transitions,[5] it is clear that tunneling studies can contribute significantly to our understanding of inorganic materials. One may ask, therefore, why little progress has been made in the analysis of electronic states by IETS. One major hindrance has been the need for better data acquisition and manipulation. Perusal of the IETS papers concerned with electronic transitions reveals that the data are acquired and displayed in d^2V/dI^2 format, they are often the result of a single scan or multiple scans of rather noisy data, and reference subtraction has not been employed. Thus, unless a large hump can be easily identified, no electronic transitions are reported.

Another problem is that much of the electronic state tunneling literature has been devoted to π to π^* transitions of large planar aromatic molecules which can significantly interact with the tunnel junction insulator or cover metal. Thus, it appeared that electronic transitions in IETS were always broad, unstructured, and often shifted in energy. Finally, because the molecule of interest may undergo chemical reaction with the oxide support used in IETS, the experimenter must be reasonably knowledgeable in his choice of support/adsorbate pair and adsorption conditions. All of these considerations relagated electronic state tunneling to an activity practiced by a few hardy souls.

We believe we have found a general solution to all (save the last) real and perceived difficulties. The present work has three objective: first, to present new data on the electronic states of $CoCl_4^{2-}$; second, to show that electronic transitions in IETS need not be broader than or shifted from electronic transitions observed optically; and finally, to describe the techniques used in obtaining high-quality electronic state spectra by IETS.

Experimental Section

Tunneling Instrumentation. The spectrometer used was recently described in the literature.[14] The d^2V/dI^2 data presented were acquired

(1) *Tunneling Spectroscopy*; Hansma, P. K., Ed.; Plenum Press: New York, 1982.
(2) Khanna, S. K.; Lambe, J. *Science* **1983**, *220*, 1345.
(3) Weinberg, W. H. *Annu. Rev. Phys. Chem.* **1978**, *29*, 115.
(4) Kirtley, J.; Hansma, P. K. *Surf. Sci.* **1977**, *66*, 125.
(5) Hipps, K. W.; Mazur, U. *Inelastic Electron Tunneling Spectroscopy*; Hansma, P. K., Ed.; Plenum Press: New York, 1982, and references therein.
(6) Hipps, K. W.; Mazur, U. *J. Phys. Chem.* **1980**, *84*, 3162.
(7) Hipps, K. W.; Williams, S. D.; Mazur, U. *Inorg. Chem.* **1984**, *23*, 3500.
(8) Hipps, K. W.; Aplin, A. T. *J. Phys. Chem.* **1985**, *89*, 5459.
(9) de Cheveigne, S.; Klein, J.; Leger, A. *Inelastic Electron Tunneling Spectroscopy*; Hansma, P. K., Ed.; Plenum Press: New York, 1982, and references therein.
(10) Adane, A.; Fauconnet, A.; Klein, J.; Leger, A.; Belin, M.; Defourneau, D. *Solid State Commun.* **1975**, *16*, 1071.
(11) Ewert, S. *Appl. Phys.* **1981**, *A26*, 63.
(12) Susla, B.; Czajka, R.; Rauluszkiewicz, J. *Phys. Status Solidi* **1983**, *120*, K129.
(13) Hipps, K. W.; Susla, B. *Chem. Phys. Lett.* **1987**, *132*, 507.

0002-7863/87/1509-3861$01.50/0

as described in ref 14. In what follows, d^2V/dI^2 data will be identified as un-normalized tunneling data. The data acquisition programs were modified for some of the data presented here, and those modifications will now be described. The first task of the data taking program was to acquire bias voltage (V)–modulation voltage (V_ω) pairs at fixed modulation current over the range of bias used in spectral data collection. This data set was then fit to an N term polynomial ($N \gtrsim 6$) and the coefficients retained. The resulting polynomial function was simply related to dV/dI. The control program then began a fixed step interval V scan in which d^2V/dI^2 data were acquired and divided in real time by the appropriate value of $(dV/dI)^2$. Thus, some of the spectra are presented as $(d^2I/dV^2)/(dI/dV)$ vs V plots which we will henceforth identify as normalized tunneling spectra. In either case, all spectra were multiply scanned and co-added to produce the final spectra.

One or more of three post-acquisition data manipulation programs were used. TUNLFIT provided a polynomial background function to be least-squares fit to selected regions of the spectrum and then the polynomial function subtracted from the entire data set. DIPFIX was used to replace the quantum size effect (QSE) structure dip[15] with a short curved line segment. SUBTUNL was used extensively for interactive data subtraction. A reference spectrum was interactively subtracted from a sample spectrum to provide the best cancellation of common bands.

For all spectra reported, the modulation voltage was set at 8 mV near 30 mV bias. Since constant modulation current was used, the modulation voltage typically fell to about 3 mV at 1 V bias. In the context of vibrational tunneling spectroscopy, these are very low resolution spectra. A 0.3 s linear time constant with 0.1 s sampling time was used. Typically 1 point was collected every 7 cm^{-1} (8.066 cm^{-1}/mV). Data were collected with the aluminum electrode biased negatively and all measurements were made at 4.2 K. In order for spectral subtraction to be effectively employed, at least 6 high-quality spectra differing in surface coverage for each type of junction were collected. Typical junction resistances ranged from 90 to 900 ohm. The spectra have been corrected for the shift induced by the superconductivity of the Pb top metal.

Tunnel Junction Fabrication. All the junctions (tunnel diodes) reported here were of the form Al–AlO_x–sample–Pb. Standard resistive deposition techniques were used to provide 1 mm wide metal strips. The oxide was grown by ac discharge in 100 μm of oxygen. Growth times were doubled for the production of reference junctions. Electrical contact was made with indium solder.

(Tetraethylammonium)cobalt(II) tetrachloride [$(Et_4N)_2CoCl_4$] was doped from ethanol with a solution concentration of 5 g/L. The reference junctions for the above were composed of a mixture of 0.3 g/L of $ZnCl_2$ and 1.2 g/L of $(Et_4N)Cl$ in ethanol. The choice of solvent was made by trading off the desire for low dielectric constant and thus high adsorption against the need for sufficient solubility. The preparation of the $CoCl_2$ doped junction from Me_2SO under inert conditions[16] and the corresponding Me_2SO reference were described elsewhere.[13]

Because the tunneling current decreases exponentially with barrier thickness, and because IETS signals do not increase significantly when the coverage exceeds 1 monolayer,[1] the spectra presented here are probably due to an average coverage of 1 monolayer and are certainly due to less than 3 monolayers.

FT–IR Data. Diffuse reflectance data of pure solid powders were obtained on an IBM IR-98 fourier transform instrument. A tungsten lamp source, a germanium coated KBr beam splitter, and a cooled InSb detector were employed. Data were acquired at 8-cm^{-1} resolution and are the result of co-adding 1024 scans. The FT–IR data presented in this paper are in Kubelka-Monk format[17] with KBr providing the reference. All spectra were obtained at room temperature. Some of the spectra are the result of interactively subtracting the spectrum of $(Et_4N)Cl$ from that of $[(Et_4N)_2CoCl_4]$ in a manner identical with that used for the subtracted tunneling spectra. It should be noted that KBr pellet spectra of this complex cannot be obtained because of halide exchange during the mixing and pressing.

Results

Figure 1 presents a typical d^2V/dI^2 spectrum obtained from the $ZnCl_2/Et_4NCl$ reference solution. For later use, please note the QSE dip near 7000 cm^{-1}. Figure 2 gives $(d^2I/dV^2)/(dI/dV)$ spectra of a typical reference junction. The lower curve is raw data. The upper curve shows the same data set after DIPFIX

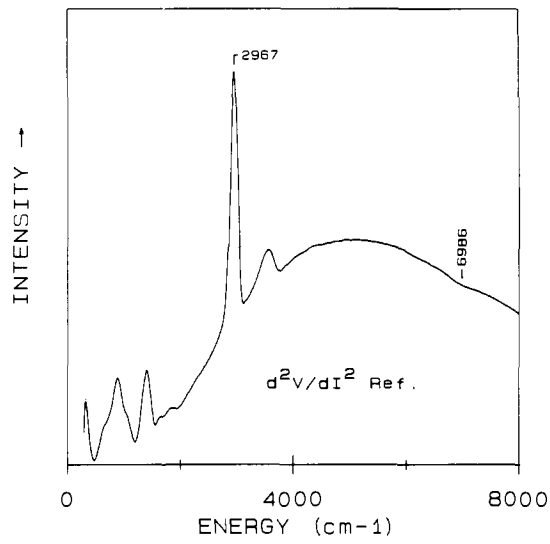

Figure 1. Non-normalized tunneling spectrum of $ZnCl_2$ + Et_4NCl reference junction having 40 co-added scans.

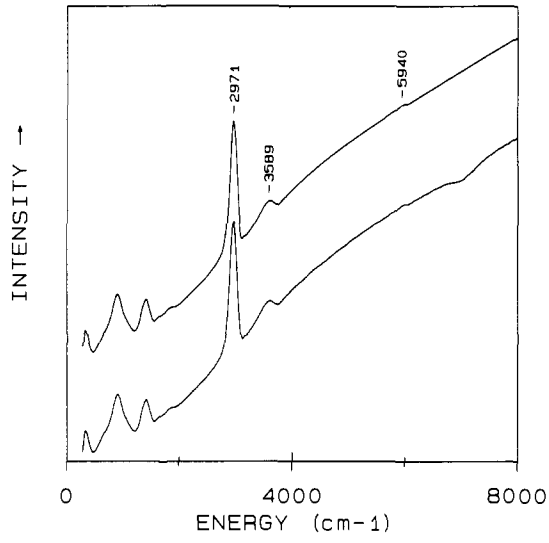

Figure 2. Normalized tunneling spectra of a $ZnCl_2$ + Et_4NCl reference junction having 74 co-added scans. The lower curve is the original data. The upper curve is the result of removing the QSE dip.

removes the QSE dip. Not that the background in Figure 2 is very regular and almost linearly increasing, while that in figure 1 requires a 6th order polynomial to approximate it.

Figure 3A presents a typical d^2V/dI^2 spectrum obtained from $(Et_4N)_2CoCl_4$. Fifty scans were co-added to produce this spectrum. Trace B presents the difference specrum obtained by interactively subtracting the spectrum of Figure 1 from that of Figure 3A. As can be seen, the peaks in different spectral regions do not subtract uniformly, and a preferred region must be chosen. In the case of Figure 3B, a subtraction factor that minimized the CH stretching band near 2970 was chosen. Note also that the plotting scale for spectrum B in Figure 3 has been chosen to magnify it by a factor of 2 relative to spectrum A in Figure 3. The peak near 1000 cm^{-1} in Figure 3B is due to incomplete subtraction of the Al–O stretch. Because the experimental sensitivity decreases with bias voltage in non-normalized spectra, optimizing the subtraction factor at the CH peak leads to larger errors at the Al–O peak. The "ringing" near 3000 cm^{-1} is due to imperfect matching of the CH band shapes in sample and reference junctions. This is a common occurrence in difference spectra (see for example, the FT–IR difference spectrum presented later).

Figure 4 is the equivalent of Figure 3 for the case of normalized spectra. Figure 4A is a $(d^2I/dV^2)/(dI/dV)$ spectrum of $(Et_4N)_2CoCl_4$ after dip removal by DIPFIX. Figure 4B is the (factor

(14) Hipps, K. W. *Rev. Sci. Instrum.* **1987**, *58*, 265.
(15) Jaklevic, R. C.; Lambe, J.; Kirtley, J.; Hansma, P. K. *Phys. Rev. B* **1977**, *15*, 4103.
(16) Hipps, K. W.; Mazur, U. *Rev. Sci. Instrum.* **1984**, *55*, 1120.
(17) Wendlandt, W. W.; Hecht, H. G. *Reflectance Spectroscopy*; International Publishers: New York, 1966; p 62.

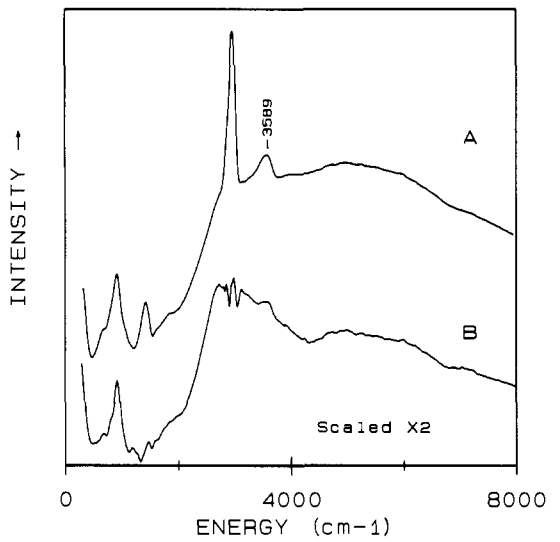

Figure 3. Non-normalized tunneling spectra of $(Et_4N)_2CoCl_4$. Trace A is the result of co-adding 50 scans. Trace B is the CH region optimized difference of spectrum A and the spectrum in Figure 1. The difference spectrum has been expanded by 2 to facilitate viewing.

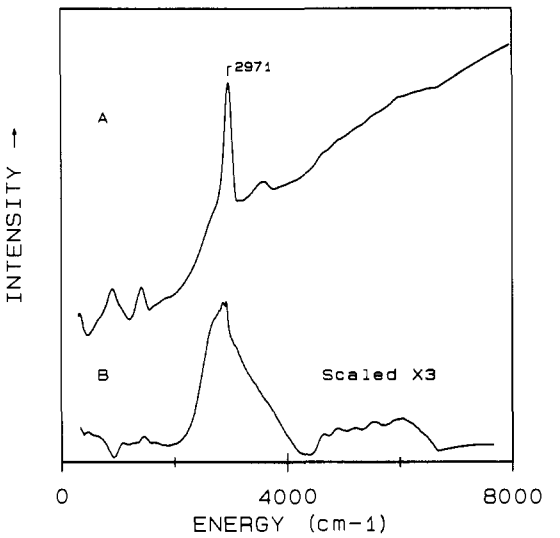

Figure 4. Normalized tunneling spectra of $(Et_4N)_2CoCl_4$. Trace A is the result of co-adding 121 scans. Trace B is the CH region optimized difference of spectrum A and the spectrum in Figure 2. The difference spectrum has been expanded by 3 to facilitate viewing.

of 3 expanded) difference spectrum obtained by subtracting the upper trace in Figure 2 from that in Figure 4A. Note that for this form of the data the subtraction efficiency is almost voltage independent and a nearly flat base line results. The Al–O band near 1000 cm^{-1} here appears as a small negative feature and the ligand bands near 1500 cm^{-1} show up as a very small positive feature. Note also that the surface OH stretching mode near 3580 cm^{-1} has been well removed from spectrum B in Figure 4 but not from spectrum B in Figure 3.

Figure 5 compares the complete diffuse reflectance spectrum of $(Et_4N)_2CoCl_4$ to the normalized tunneling spectrum. The upper trace is the spectrum of Figure 4A after subtraction of a smooth base line function. The peak intensity of the FT–IR spectrum is 2.8. Figure 6 is a similar presentation of cation-corrected spectra. The solid curve represents the difference spectrum obtained when the FT–IR spectrum of Et_4NCl is subtracted from that of $(Et_4N)_2CoCl_4$. The broken line is simply an expanded plot of Figure 4B.

Figure 7 and Table I present detailed views of the 4000–7500-cm^{-1} region of the $(Et_4N)_2CoCl_4$ tunneling and FT–IR spectra. The upper two plots are cation corrected data taken from Figure 6. The lower plot was obtained by fitting a low-order

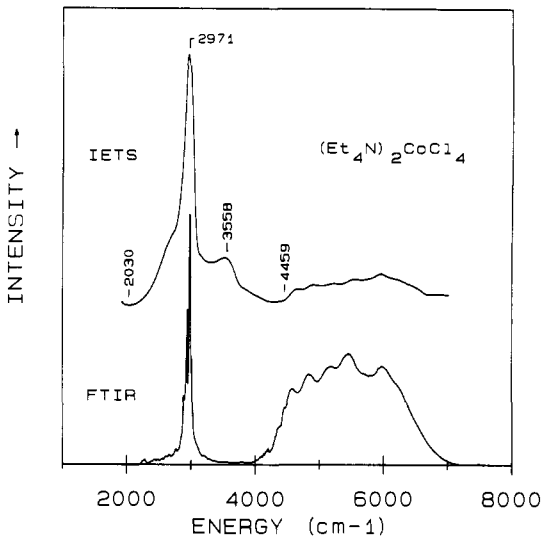

Figure 5. Spectra of $(Et_4N)_2CoCl_4$. The lower trace is the diffuse reflectance FT–IR spectrum and the upper trace is a portion of Figure 4A after subtracting a low-order polynomial to provide a flat base line.

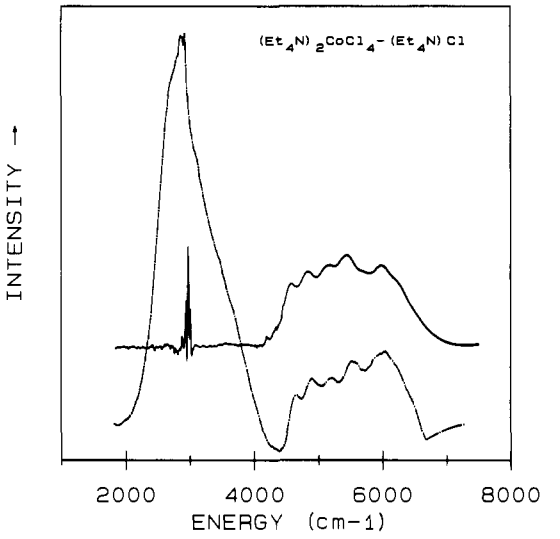

Figure 6. Cation corrected spectra of $(Et_4N)_2CoCl_4$. The broken curve is an expanded view of Figure 4B. The solid curve is the result of interactively subtracting the diffuse reflectance FT–IR spectrum of Et_4NCl from that of $(Et_4N)_2CoCl_4$.

Table I. Peak Positions (cm^{-1}) of the Structure in the $^4A_2 \rightarrow {}^4T_1$ Transition as Observed by FT–IR and IETS

FT–IR[a]	IETS-A[b]	IETS-B[b]
4580	4653	4655
4841	4893	4898
5180	5198	5196
5452	5525	5517
5709 (sh)	5700 (sh)	5780 (sh)
5990	5985	5940
6237 (sh)	6235 (sh)	6230 (sh)

[a] The uncertainty is ±10 cm^{-1}. [b] The uncertainty is ±15 cm^{-1}.

polynomial to the background of the $(Et_4N)_2CoCl_4$ normalized tunneling spectrum and then subtracting that polynomial. No dip removal or reference spectrum subtraction was employed. Table I presents the approximate peak positions of the features in Figure 7.

Figure 8 contrasts the reference subtracted tunneling data obtained in the 4000–7500-cm^{-1} region from junctions prepared in very different manners. The upper spectrum was first reported by Hipps and Susla[13] and is the result of inert atmosphere doping with $CoCl_2$ in Me_2SO solution. The lower curve is a tunneling spectrum of $(Et_4N)_2CoCl_4$ doped from ethanol in air.

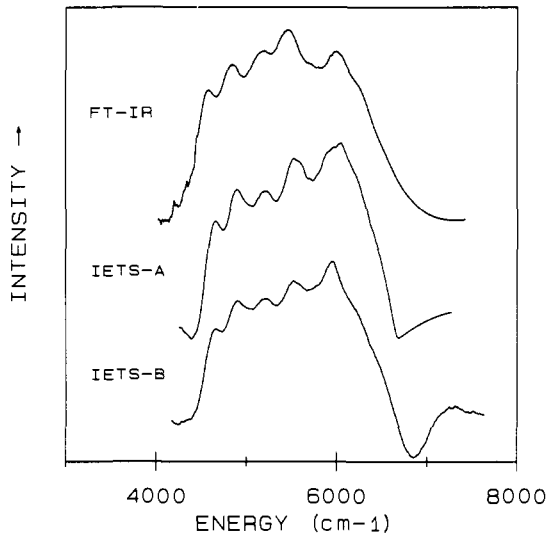

Figure 7. Spectra of the $^4A_2 \rightarrow {}^4T_1$ transition of $(Et_4N)_2CoCl_4$. The upper two curves are corresponding segments taken from Figure 6. The lower curve is the result of subtraction of a smooth background function from the original sample data without any spectral subtraction or dip removal.

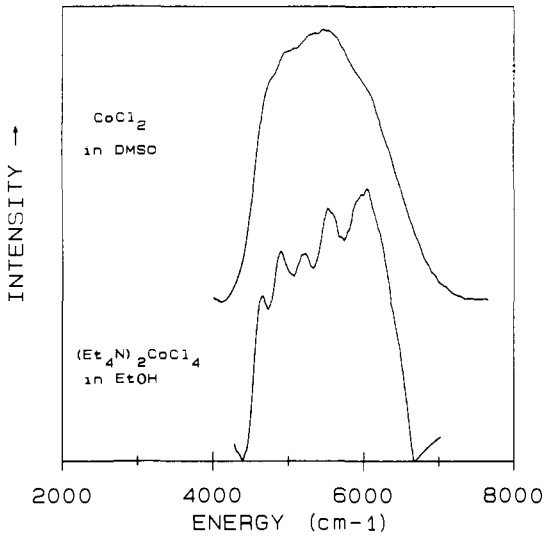

Figure 8. Comparison of the $^4A_2 \rightarrow {}^4T_1$ transition region of $(Et_4N)_2CoCl_4$ and $CoCl_2$ doped tunnel junction spectra.

Discussion

Data Presentation. Review of Figures 1–4 clearly demonstrates that normalized tunneling data are far superior to d^2V/dI^2 data for use in either reference or background subtraction. The normalized data can provide a uniform subtraction of common features to yield a nearly flat base line in the rapidly varying vibrational region of the spectrum. Thus, one can give very high confidence to features seen above 4000 cm^{-1} where the reference junctions are nearly featureless. In contrast, even the best matched d^2V/dI^2 spectra do not give flat base lines. It should be stressed here, however, that good base lines for subtracted data are contingent on the selection of an appropriate reference. If Et_4NCl solutions are used without $ZnCl_2$, for example, the quality of the difference spectra is quite poor. Thus, there are two elements required for successful spectral subtaction of tunneling data. Normalized spectra should be used and the reference concentration, composition, and oxide thickness must be varied to produce a good match to the sample spectrum. If simple background subtraction (polynomial fitting) is used, the nearly linear background present in normalized tunneling spectra make the procedure far more accurate than for the highly curved background in d^2V/dI^2 spectra.

In this context, we should note that the standard practice to date in identifying electronic transitions by IETS has been to simply draw an assumed extension of the elastic background under the proposed electronic transition. While this procedure works for strong transitions in an otherwise empty region of the spectrum (compare parts A and B in Figure 7), it works quite poorly for the strong broad feature extending from 2000 to 4000 cm^{-1}. Spectral subtraction techniques used on normalized spectra, however, work very well indeed (see Figure 4B).

Spectral (reference) subtraction works so well that the primary problem becomes removing the QSE dip. Unlike vibrational or electronic structure, the QSE dip varies in position, depth, and form with temperture, strain, Pb thickness, and other variables.[15] Thus it is almost impossible to remove by spectral subtraction, often producing a large derivative-like structure in the difference spectrum. Our as yet incomplete solution to this problem has been to replace the QSE dip area with a short curved line segment. This works great for junctions having no other features in the vicinity of the dip (see Figure 2), but it is not quite satisfactory when bands overlap it. The lower two traces of Figure 7, and the data in Table I, show how the data are changed with partial QSE removal and spectral subtraction. We are presently working on a more sophisticated method of QSE dip removal.

Spectral Assignments. We next turn our attention to assigning the electronic transitions in the cobalt(II) tetrachloride spectra. First consider the well-structured band centered on 5550 cm^{-1}. The structure observed on this band is a clear indication that it is an electronic transition. Its intensity in the IR is clearly consistent with an allowed d–d transition. Moreover, its location is in good agreement with the reported positions of $^4A_2 \rightarrow {}^4T_1$ d–d transitions in tetrahedral $CoCl_4^{2-}$ in solution and solid phase.[18-20] Thus, the 4400–6600-cm^{-1} feature is confidently assigned to the $^4A_2 \rightarrow {}^4T_1$ transition in tetrahedral $CoCl_4^{2-}$. Further, considering the difference in measurement temperature (300 K vs. 4 K) the agreement in the structure seen in IETS and FT–IR is excellent (see Figure 7 and Table I). Thus the environment of the ion inside the tunnel junction is quite similar to that in the solid tetraethylammonium salt.

As is easily seen from Figure 6, the very intense broad band centered near 3000 cm^{-1} in the IETS has no counterpart in the FT–IR spectrum. If it is due to an electronic transition, it must be due to a dipole-forbidden one. Consideration of the states of the $CoCl_4^{2-}$ ion[18-22] indicates that there is a single term having energy between the ground term ($^4A_2$) and the $^4T_1$ term—the $^4T_2$. Taking the position of the allowed transition as 5500 cm^{-1}, one may calculate[21] the expected band maximum of the dipole-forbidden $^4A_2 \rightarrow {}^4T_2$ transition to lie near 3080 cm^{-1}, in excellent agreement with the observed tunneling band. Further, the widths of both transitions are consistent with experimental and theretical observations.[18-22] Thus, the two strong bands observed in the tunneling difference spectrum (Figure 6) are due to electronic transitions of tetrahedral cobalt(II) tetrachloride.

In a recent letter,[13] we assigned the strong broad bands observed in the spectrum of $CoCl_2$-doped tunnel junctions to the electronic transitions of the $CoCl_4^{2-}$ ion. The comparison of the 5500-cm^{-1} bands presented in Figure 8 now confirms this assignment. The difference in structuring of the bands is certainly due to environmental influences. In the case of $CoCl_2$-doped junctions, surface Al^{3+} ions must serve as the counterions for the surface formed cobalt tetrachloride ions.

Intensities and Band Shapes. Figures 5 and 6 provide interesting contrasts in the IETS and FT–IR selection rules. Most obviously, the integrated intensity of the dipole-forbidden transition in the IET spectrum is greater than that of any other band in that spectrum. Even in the case of bands that are allowed in both techniques, there are significant inensity differences. For example,

(18) Cotton, F. A.; Goodgame, D. M.; Goodgame, M. *J. Am. Chem. Soc.* **1961**, *83*, 4690.
(19) Weakliem, H. A. *J. Chem. Phys.* **1962**, *36*, 2117.
(20) Ferguson, J. *J. Chem. Phys.* **1963**, *39*, 116.
(21) Ballhausen, C. J.; Liehr, A. D. *J. Mol. Spectrosc.* **1958**, *2*, 342.
(22) Furuhashi, H.; Inagaki, M.; Naka, S. *J. Inorg. Nucl. Chem.* **1973**, *35*, 3009.
(23) Igalson, J.; Adler, J. G. *Phys. Rev. B* **1983**, *28*, 4970.

if the CH stretching (near 2970 cm^{-1}) peak height is chosen as a normalizing factor, the $^1A_2 \rightarrow {}^4T_1$ d-d transition is a factor of 2 or 3 weaker in the IETS than in FT-IR. There are also a number of combination bands near 4000 cm^{-1} in the FT-IR spectrum which do not appear in the tunneling spectrum.

Perhaps the most important single feature of this work is the observation of well-defined structure on an electronic transition by tunneling spectroscopy. The spectra presented here very clearly show that shifts and broadening of electronic transitions in IETS are most probably due to chemical interactions between the tunnel junction insulator or top metal and the sample. Tunneling is intrinsically capable of yielding good quality electronic spectra! This will be further emphasized in a future publication concerning the electronic tunneling, FT-IR, and Raman spectra of a series of cobalt complexes.[24]

A minor but interesting point relates to the very weak band near 5940 cm^{-1} in Figure 2. This is almost certainly an overtone of the 2970 cm^{-1} CH stretch. It is our belief that overtones and combination bands are very very weak in IETS. Even the often quoted Al-O overtone assignment has been severely questioned.[23] Thus the observation of an overtone, even for a strong band such as the CH stretch, is novel in our experience.

(24) Hipps, K. W.; Mazur, U., work in progress.

Conclusions

Tunneling spectroscopy is a viable electronic spectroscopy for studying transitions occurring in the IR and near-IR region of the spectrum. Vibronic and/or spin-orbit structuring of electronic transitions may be observed with quality similar to that found in room temperature optical spectroscopy. The selection rules are such that spin- and dipole-forbidden transitions may be observed with significant intensity.

Many of the problems associated with generalizing tunneling to allow the study of low-lying electronic transitions in arbitrary molecular systems have been solved. The remaining major hurdle is posed by the structure of the commonly used tunnel junctions. The production of reliable junctions having less reactive insulators would eliminate the last barrier to complete generalization of IETS to electronic spectroscopy in the IR and near-IR region of the spectrum.

Acknowledgment. We gratefully acknowledge the National Science Foundation and the Division of Materials Research for their support in the form of Grants DMR-8414566 and DMR-8320556. We also thank A. T. Aplin and S. N. Sarkar for their valued assistance.

Metalloporphyrin Core Size Resonance Raman Marker Bands Revisited: Implications for the Interpretation of Hemoglobin Photoproduct Raman Frequencies

N. Parthasarathi, C. Hansen, S. Yamaguchi, and T. G. Spiro*

Contribution from the Department of Chemistry, Princeton University, Princeton, New Jersey 08544. *Received October 17, 1986*

Abstract: Resonance Raman frequencies are examined for high-frequency skeletal modes of several metalloprotoporphyrin derivatives. The previously noted inverse dependence on core size applies to Mn, Co, and Zn as well as to Fe and Ni species, and slightly revised coefficients are derived from the expanded data base. Systematic deviations are noted for 2-methylimidazole adducts of Mn^{II}, Fe^{II}, and Co^{II} and are suggested to be associated with electronic effects of porphyrin doming, or of tilting of the metal-ligand bond relative to the porphyrin plane. Positive deviations are seen for Cl_2Sn^{IV}; evidently the correlations break down for so large a central ion (C_t-N = 2.082 Å). A core-size dependence is also noted for ν_4, the "oxidation-state marker" for heme proteins, but the slope is much smaller than for the higher frequency skeletal modes, accentuating the negative deviations seen for Fe^{II}, and also Mn^{II} and CO^{II} derivatives; other M^{II} derivatives (Ni, Zn) fall on the line, so there appears to be an electronic basis for the oxidation-state dependence, over and above the core-size dependence. Significantly, the core-size dependence is obeyed for $[(OH)_2Fe(PP)]^{2-}$, a six-coordinate but high-spin Fe^{II} species. This observation establishes a base line for the core-size analysis of the RR frequencies of the early photolysis product of CO-hemoglobin (Hb) and their shifts relative to deoxyHb. The present results are consistent with the most recent interpretation, that the Fe is out of the heme plane in the photoproduct, but not by as much as in deoxyHb. Core-size correlations are also found for metallo TPP's, but the coefficients differ from those of metallo PP's reflecting the altered normal mode compositions.

Because heme resonance Raman (RR) frequencies show marked sensitivity to redox and ligation state and to the nature of the surrounding protein,[1] there has been strong interest in trying to establish the structural basis of these dependencies via systematic studies of metalloporphyrins. Spaulding et al.[2] first noted a dependence of one of the high-frequency RR bands on the size of the central cavity in a series of structurally determined metallo octaethylporphyrins, and Huong and Pommier[3a] found a core-size dependence for two other bands as well, as did Spiro et al.,[3b] who analyzed relative effects of core size and doming on these frequencies. In 1982 Choi et al. were able to assign the protoporphyrin (PP) RR spectrum[4] and to track the modes for a series of Fe derivatives as well as NiPP.[5] They found that all the skeletal (but not peripheral vinyl) modes above 1450 cm^{-1} showed an inverse linear correlation with core size, and attributed this effect

(1) (a) Spiro, T. G. In *Iron Porphyrins*, Part II; Lever, A. B. P., Gray, H. B., Eds.; Addison-Wesley: Reading, MA, 1983; pp 89-160. (b) Spiro, T. G. *Adv. Protein Chem.* **1985**, *37*, 111-159. (c) Kitagawa, T.; Ozaki, Y. *Struct. Bonding (Berlin)*, in press.

(2) Spaulding, L. D.; Chang, C. C.; Yu, N-T.; Felton, R. H. *J. Am. Chem. Soc.* **1975**, *97*, 2517.

(3) (a) Huong, P. V.; Pommier, J.-C. *C. R. Acad. Sci., Ser. C* **1977**, *285*, 519. (b) Spiro, T. G.; Stong, J. D.; Stein, P. J. *J. Am. Chem. Soc.* **1979**, *101*, 2648.

(4) Choi, S.; Spiro, T. G.; Langry, K. C.; Smith, K. M. *J. Am. Chem. Soc.* **1982**, *104*, 4337.

(5) Choi, S.; Spiro, T. G.; Langry, K. C.; Smith, K. M.; Budd, L. D.; LaMar, G. N. *J. Am. Chem. Soc.* **1982**, *104*, 4345.

0002-7863/87/1509-3865$01.50/0